RESEARCH ARTICLE OPEN ACCESS

Cognitive Impairment in a Complex Family With AAGGG and ACAGG Repeat Expansions in RFC1 Detected by ExpansionHunter Denovo

Kazuki Watanabe, MD, Mitsuko Nakashima, MD, PhD, Rie Wakatsuki, MD, Tomoyasu Bunai, MD, PhD, Yasuomi Ouchi, MD, PhD, Tomohiko Nakamura, MD, PhD, Hiroaki Miyajima, MD, PhD, and Hirotomo Saitsu, MD, PhD

Correspondence
Dr. Saitsu
hsaitsu@hama-med.ac.jp

Neurol Genet 2022;8:e682. doi:10.1212/NXG.0000000000000682

Abstract

Background and Objectives

We investigated the genetic basis and brain metabolism and blood flow of a Japanese family with spinocerebellar degeneration (SCD), with multiple affected members for 3 generations.

Methods

After excluding DNA repeat expansion (RE) of common SCD genes by fragment analysis, we performed whole-exome sequencing (WES) and whole-genome sequencing (WGS). Homozygosity mapping was performed using these data. REs were investigated with WGS data using ExpansionHunter Denovo and Expansion Hunter.

Results

WES and WGS were unable to identify likely pathogenic variants, and homozygosity mapping failed to narrow down the locus. However, ExpansionHunter Denovo detected REs in intron 2 of the *RFC1* gene and led us to the diagnosis of *RFC1*-related disorders. Subsequent repeat-primed PCR and Southern blot hybridization analyses revealed that 3 of 6 patients and 1 suspected individual had expansions of AAGGG ($(AAGGG)_{exp}$) and $(ACAGG)_{exp}$ repeats in a compound heterozygous state and 3 had a homozygous $(ACAGG)_{exp}$. The patients showed a variety of clinical features, including adult-onset ataxia, sensorimotor neuropathy, head tremor, parkinsonism, dystonia, and cognitive impairment. A comparison of previous reports with those of the family in study suggested that motor neuropathy could be a feature of compound heterozygous patients and biallelic $(ACAGG)_{exp}$ patients. Cognitive function tests showed cognitive impairment with a predominance of frontal lobe dysfunction. Examination of MRI, SPECT, and ^{18}F-fluorodeoxyglucose-PET showed clear cortical damage with frontal lobe predominance in 1 case, but no cerebral damage was evident in the other 2 cases.

Discussion

Our report shows the usefulness of WGS and RE detection tools for SCD of unknown cause. The studied family with *RFC1*-related disorders included patients with $(ACAGG)_{exp}$ and $(AAGGG)_{exp}$ in a compound heterozygous state and was characterized by motor neuropathy. Based on the results of cognitive function tests and imaging studies, 1 patient presented with cognitive impairment due to frontal lobe metabolic changes, but there were also patients who presented with cognitive impairment without apparent cerebral metabolic or blood flow, suggesting that other factors are also associated with cognitive impairment.

From the Department of Biochemistry (K.W., M.N., H.S.), Department of Neurology (K.W., R.W., T.B., T.N., H.M.), and Department of Biofunctional Imaging (T.B., Y.O.), Hamamatsu University School of Medicine, Hamamatsu, Japan.

Go to Neurology.org/NG for full disclosures. Funding information is provided at the end of the article.

The Article Processing Charge was funded by the authors.

Glossary

CANVAS = cerebellar ataxia, neuropathy, and vestibular areflexia syndrome; **CCAS** = cerebellar cognitive affective syndrome; **DIG** = digoxigenin; **EHdn** = ExpansionHunter Denovo; **FAB** = frontal assessment battery; **^{18}F-FDG** = ^{18}F-fluorodeoxyglucose; **MMSE** = Mini-Mental State Examination; **RE** = repeat expansion; **RP-PCR** = repeat-primed PCR; **SCA** = spinocerebellar ataxia; **SCD** = spinocerebellar degeneration; **VSRAD** = voxel-based specific regional analysis system for Alzheimer disease; **WES** = whole-exome sequencing; **WGS** = whole-genome sequencing.

Spinocerebellar degeneration (SCD) is a heterogeneous group of diseases, with ataxia being the core symptom caused by the degeneration of the cerebellum or its connecting pathways, and includes many diseases resulting from genetic abnormalities. Expansion of short tandem repeats (repeat expansions, REs) is a common cause of hereditary SCD, and repeat-primed PCR and fragment analysis have been widely used to detect REs.[1] However, because these techniques cannot comprehensively detect REs, the demand for a comprehensive method to detect REs has increased. Along with long-read sequencing, which is quite powerful for detecting REs,[2] several RE detection tools using short-read sequencing data have been recently developed,[3] including Expansion Hunter and ExpansionHunter Denovo (EHdn). However, there are still few reports on detection of REs using these tools.[4–7]

Cerebellar ataxia, neuropathy, and vestibular areflexia syndrome (CANVAS) is a rare hereditary disease characterized by progressive late-onset ataxia, sensory axonal neuropathy, and bilateral vestibulopathy, which was first described in the 1990s[8,9] and is caused by a biallelic AAGGG RE in intron 2 of the *RFC1* gene.[10] Biallelic ACAGG RE was also found to be a cause of CANVAS in 2020,[11] and the ACAGG and AAGGG REs are thought to have arisen from a single origin because they share the same conserved core haplotype.[11] Because the causative gene has been identified, the detailed symptoms and new symptoms are now characterized more extensively, and there are reports showing the clinical form of multiple system atrophy,[12,13] dopa-responsive parkinsonism,[14] cognitive impairment,[15,16] chorea, and dystonia.[15] *RFC1*-related disorders are considered a spectrum of disorders with variable combinations of 5 core features: cerebellar ataxia, sensory neuropathy, vestibulopathy, cough, and autonomic dysfunction that transcends the framework of CANVAS.[15]

Here, we report a Japanese family with *RFC1*-related disorders, with multiple affected members for 3 generations. Although it was difficult to make a diagnosis based on clinical symptoms because of a wide variety of atypical clinical manifestations and to identify the locus because of the complex family structure, RE detection by whole-genome sequencing (WGS) and subsequent analysis revealed that 3 of 6 patients and 1 suspected individual had AAGGG expansion ($(AAGGG)_{exp}$) and $(ACAGG)_{exp}$ in a compound heterozygous state, and 3 had homozygous $(ACAGG)_{exp}$. A detailed comparison of clinical findings with previous reports of homozygous RE of AAGGG and ACAGG, and consideration of brain imaging and cognitive impairment, is shown in the present study.

Methods

Standard Protocol Approvals, Registrations, and Patient Consent

This study was approved by the Institutional Review Board Committee of Hamamatsu University School of Medicine (approval no. 19-339, 2020/03-02). Written informed consent was obtained from the participants before the study, and consent to use information and samples of the deceased individuals was obtained from the family.

Participants

A total of 11 Japanese individuals (6 affected, 4 unaffected, and 1 suspected individual), belonging to a village in Japan and distantly related, participated in this study (Figure 1). Spinocerebellar ataxia (SCA) types 1, 2, 3, 6, 7, 8, 10, and 17 as well as dentatorubral-pallidoluysian atrophy and Friedreich ataxia were excluded by fragment analysis.

Clinical Evaluation

We collected all clinical data from clinical assessments. To assess brain atrophy, we analyzed 3D T1-weighted MRI images of 3 patients (III-9, III-11, and IV-9) using voxel-based specific regional analysis system for Alzheimer disease (VSRAD) software (VSRAD Advance 2) (Eisai, Tokyo, Japan). Three-dimensional stereotactic surface projections were used to analyze the results of N-isopropyl-^{123}I-ρ-iodoamphetamine SPECT and ^{18}F-fluorodeoxyglucose (^{18}F-FDG) PET, which were performed in 2 patients.

Next-Generation Sequencing

Genomic DNA was isolated from blood using standard techniques. We used the DNA of deceased individuals, which was obtained for genetic testing before this study and then stored at our facility. Whole-exome sequencing (WES) was performed on 5 affected individuals (III-7, III-8, III-9, III-11, and IV-9) and 2 unaffected individuals (III-10 and III-12), and WGS was performed on III-9, III-11, and III-12. For WES, DNA was captured using an xGen Exome Research Panel kit (IDT, San Diego, CA) and sequenced on a NextSeq500 (Illumina, San Diego, CA) with 75-bp paired-end reads. For WGS, DNA was sequenced on a DNBSEQ-T7 (MGI Tech, Shenzhen, China) with 150-bp paired-end reads. Reads were

Figure 1 Pedigree Chart of the Families Who Participated in This Study

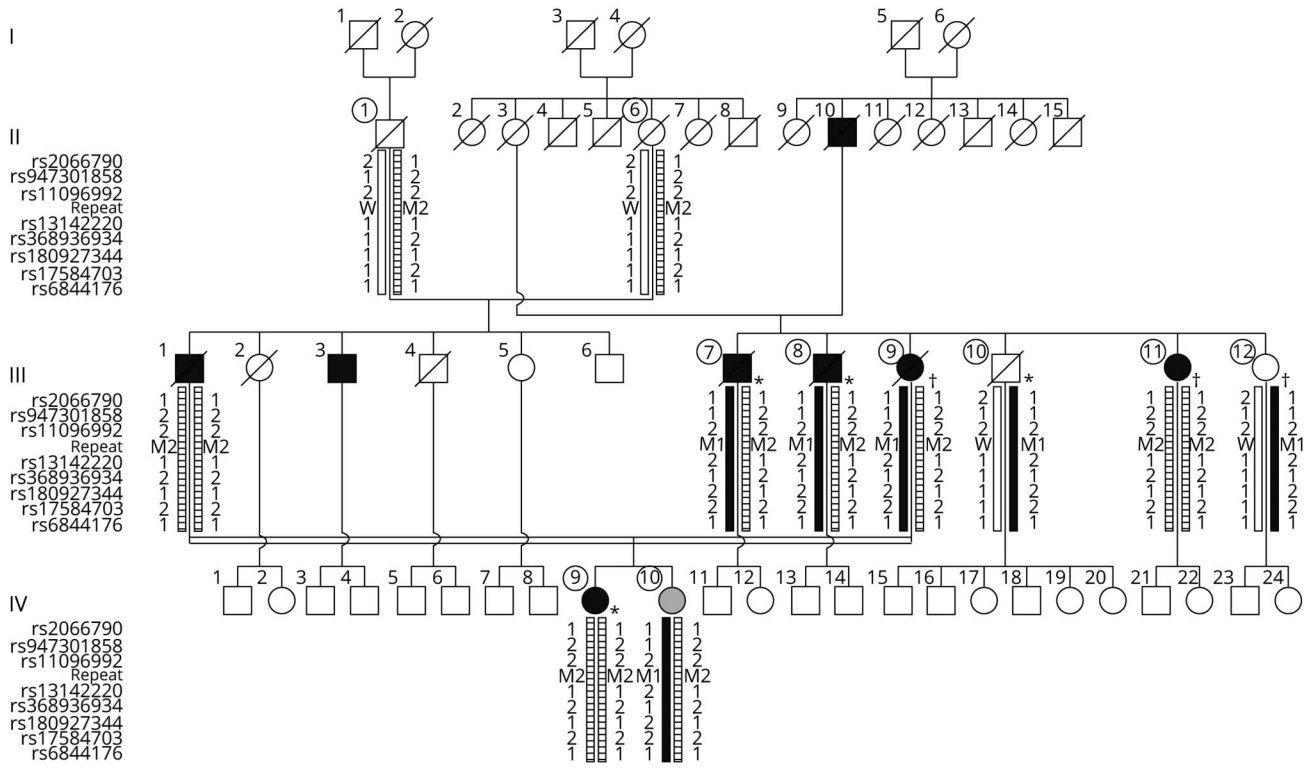

Open symbols represent nonaffected individuals, filled in symbols affected individuals, and the gray symbol an individual with suspected disease. The circles around the numbers represent the people from whom DNA was obtained. * represents those for whom WES was performed, and † represents those for whom both WES and WGS were performed. The bars and numbers next to them indicate the haplotypes associated with the motifs of repeats. The color of the bars reflects the repeat motif: white indicates $(AAAAG)_{exp}$, black indicates $(AAGGG)_{exp}$, and horizontal stripes indicate $(ACAGG)_{exp}$. The number next to the bar represents the genotype of the SNVs, and the genotypes are expressed as 1 for the reference allele and 2 for the minor allele. M1, M2, and W represent the genotypes of the repeats, with M1 representing $(AAGGG)_{exp}$, M2 representing $(ACAGG)_{exp}$, and W representing $(AAAAG)_{exp}$. SNV = single nucleotide variant; WES = whole-exome sequencing; WGS = whole-genome sequencing.

aligned to the reference genome (GRCh38) using BWA-MEM (version 0.7.17). Duplicated reads were removed using Picard (version 2.20.3), and local realignment and base quality recalibration were performed using GATK (version 3.8.1). Variants were identified using GATK HaplotypeCaller. The final variants were annotated with Annovar to predict the functional impact of the coding variants and to assess allele frequency using the following databases: an in-house database of 218 control exomes, the Human genetic variation database,[17] the ToMMo 8.3KJPN[18] allele frequency panel, and the gnomAD[19] database. We focused on rare variants with minor allele frequencies below 1% in the 4 databases. Damage prediction was performed using SIFT,[20] PolyPhen-2,[21] MutationTaster,[22] and CADD[23] programs. The eXome-Hidden Markov Model,[24] relative depth of coverage ratios,[25] and Canvas Copy Number Variant Caller[26] were used to detect the copy number variant. Structural variants and mobile element insertions were detected using the Manta Structural Variant Caller[27] and Mobster,[28] respectively.

Homozygosity Mapping

Homozygosity mapping was performed using HomozygosityMapper[29] using WES data.

Detection of REs

To detect REs, EHdn v0.9.0[30] and ExpansionHunter[31] were performed using default parameters. EHdn can detect REs across the entire genome without the need for specifying the location of REs in advance.[30] After identification of $(ACAGG)_{exp}$ by EHdn, Expansion Hunter was used to confirm the $(ACAGG)_{exp}$ in *RFC1*.

Flanking PCR and Repeat-Primed PCR

We performed flanking PCR to confirm the presence of REs in intron 2 of *RFC1* using primers used in a previous study.[10] We then performed repeat-primed PCR (RP-PCR) for AAGGG, ACAGG, AAAGG, and AAAAG repeats to determine the motif of the repeat using the same primers used in previous studies.[10,11]

Southern Blot Hybridization Analysis

A total of 10 μg of DNA was digested by *Eco*RI (New England Biolabs, Ipswich, MA) for 16 hours, and then, samples were electrophoresed on a 1% agarose gel for 8 hours at 50 V together with GeneRuler 1 kb Plus DNA Ladder (Thermo Scientific, Waltham, MA). After recording the position of the DNA ladder, the lane of the DNA ladder was removed. The remaining gel was depurinated in 0.25 M HCl for 15 minutes

Figure 2 Results of Repeat Searches Using the Repeat Expansion Detection Tools

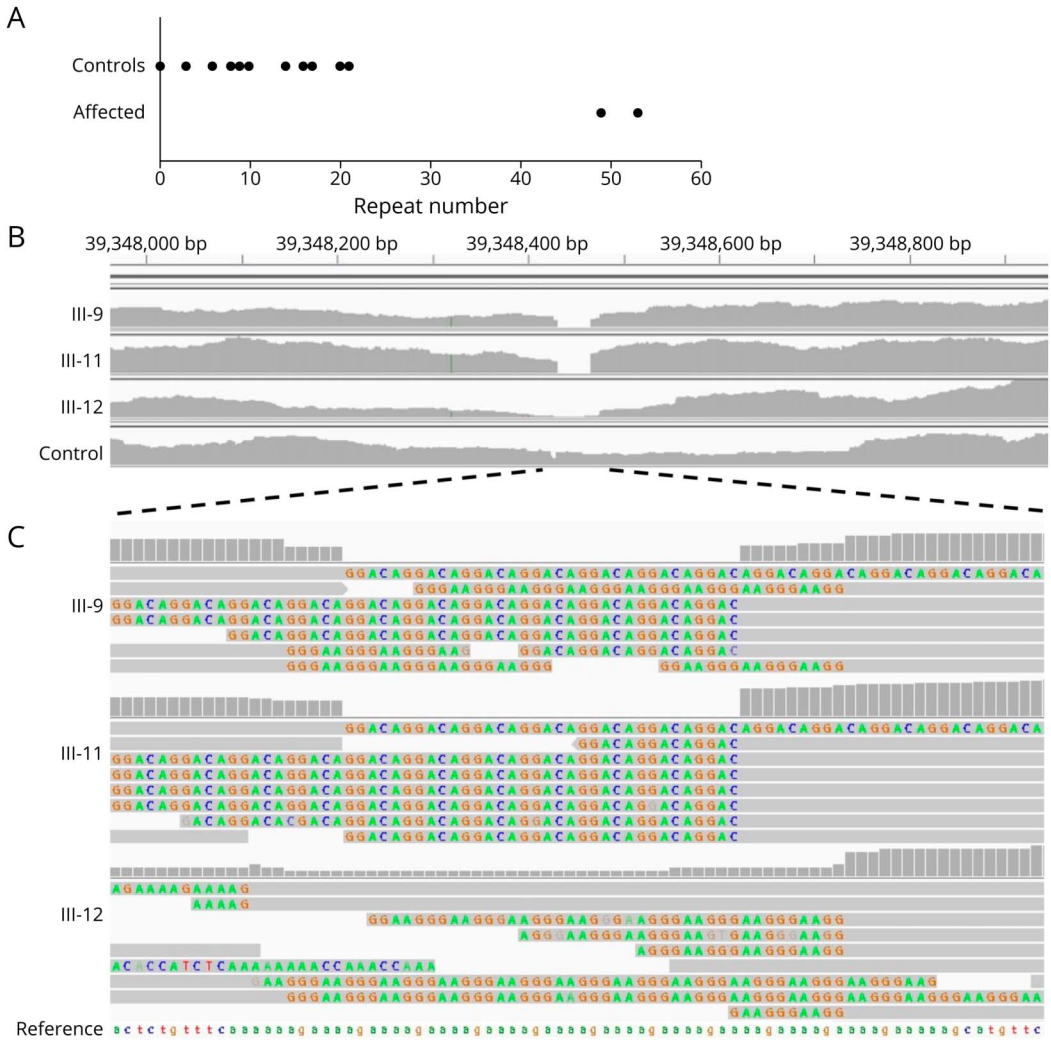

(A) Graph of Expansion Hunter results for ACAGG repeats. The data suggest an increase in the number of repeats in affected individuals III-9 and III-11 compared with those in the 28 controls. (B) The depth of aligned reads in *RFC1* was visualized by Integrative Genomics Viewer. There are clear gaps in the repeat region of *RFC1* in affected III-9 and III-11, and the depth was lowered in unaffected III-12 compared with a control individual. (C) The sequences of the soft-clipped reads showed repeats of AAGGG and ACAGG in III-9, ACAGG in III-11, and AAGGG and AAAAG in III-12.

and denatured in 0.4 M NaOH/0.6 M NaCl for 30 minutes. DNA fragments were transferred to a positively charged nylon membrane (Cytiva, Marlborough, MA) by capillary blotting. The digoxigenin (DIG)-labeled probe was created by PCR using the PCR DIG Probe Synthesis Kit (Roche Applied Science, Penzberg, Germany) using fragments of genomic DNA cloned into the pGEM-T Easy Vector (Promega, Madison, WI) as templates. Primer pairs used for the cloning of the gDNA fragment and PCR amplification of the DIG-labeled probe were the same as those used in a previous study.[10] After prehybridization at 46°C in DIG Easy Hyb (Roche Diagnostics, Basel, Switzerland) for 30 minutes, the membrane was hybridized at 46°C for 16 hours in 5 mL of DIG Easy Hyb containing 10 μL of DIG-labeled probe. The membrane was washed twice with 0.1% sodium dodecyl sulfate/2X standard sodium citrate for 5 minutes and then washed twice with 0.1% sodium dodecyl sulfate/0.5X standard sodium citrate at 65°C for 15 minutes. For detection of the DIG-labeled hybridized probe, CDP-Star (Roche Diagnostics) was used as a chemiluminescent substrate. Chemiluminescence was detected using FUSION FX7.EDGE (M & S Instruments, Osaka, Japan). The size of each band was determined by measuring the length of each band from the edge of the membrane and comparing it to the location of the marker that had been recorded. The number of repeats was calculated from the difference in size between each band and the wild-type band.

Haplotype Analysis

We investigated variants around *RFC1* to confirm the conservation of the previously reported ancestral core haplotype[10,11] associated with REs using WGS data of III-9, III-11, and III-12. We confirmed the genotypes of each single nucleotide variant by Sanger sequencing for individuals whose data were not subjected to WGS.

Figure 3 Results of Flanking PCR, RP-PCR, and Southern Blot Hybridization Analysis

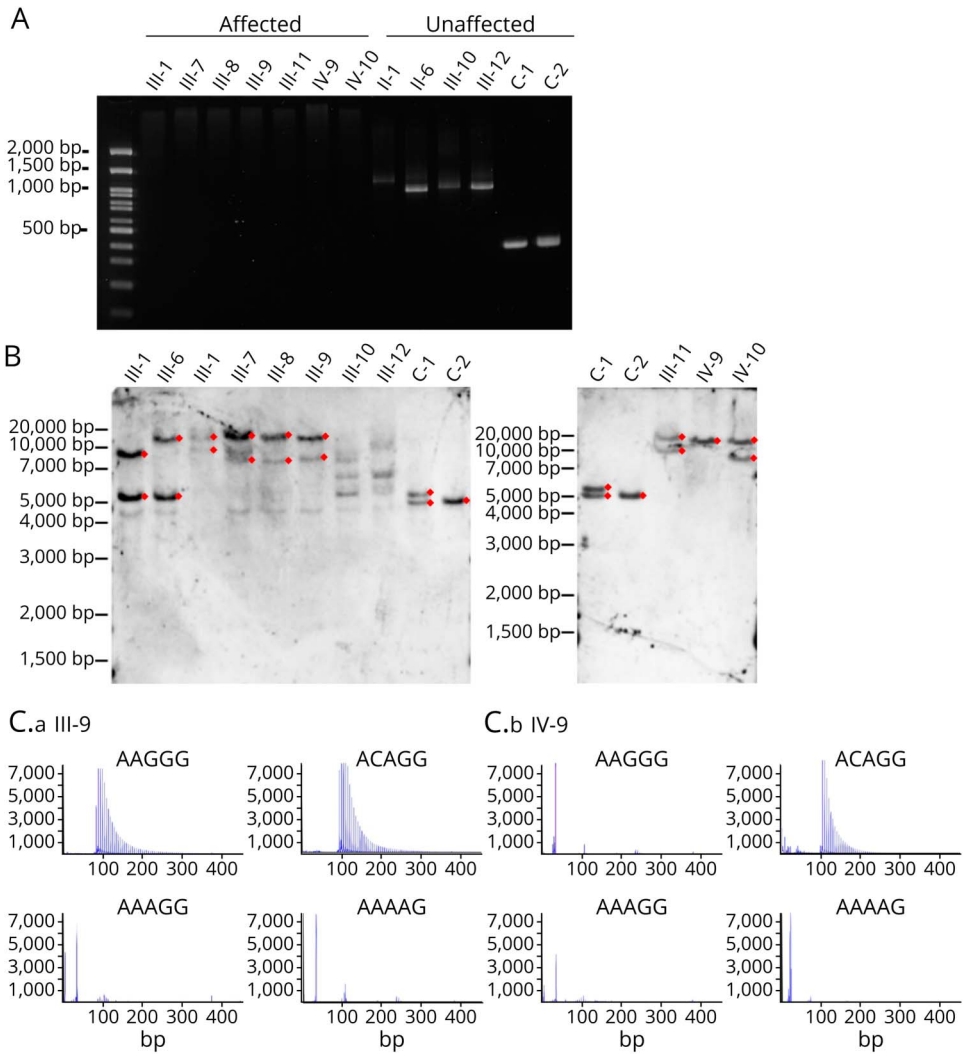

(A) The flanking PCR showed a fragment of 348-bp in healthy controls (C-1 and C-2) but could not amplify any fragments in affected individuals (III-1, III-7, III-8, III-9, III-11, IV-9, and IV-10), which suggests that there were biallelic repeat expansions. In unaffected individuals (II-1, II-6, III-10, and III-12), bands were observed around 900–1,000 bp, suggesting that there was at least 1 intermediate repeat expansion. (B) Southern blot hybridization analysis using genomic DNA from 6 patients, 1 suspected individual, and unaffected relatives probed with DIG. The target bands were marked with a red diamond. In the experiment shown on the left, genomic DNA that has been stored for a long time was used. Patients (III-1, III-7, III-8, III-9, III-11, and IV-9) and a suspected individual (IV-10) showed either 2 bands or 1 overlapping band much longer than 5 kb. Unaffected individuals (II-1 and II-6) and controls (C-1 and C-2) showed at least 1 band of approximately 5 kb in size. The target bands were unclear in III-10 and III-12. (C.a-b) Representative examples of RP-PCR targeting pathologic $(AAGGG)_{exp}$ and $(ACAGG)_{exp}$ and nonpathologic $(AAAGG)_{exp}$ and $(AAAAG)_{exp}$ in III-9 (C.a) and IV-9 (C.b). III-9 was positive for $(AAGGG)_{exp}$ and $(ACAGG)_{exp}$ in a compound heterozygous state, and IV-9 was positive for $(ACAGG)_{exp}$. DIG = digoxigenin; RP-PCR = repeat-primed PCR.

Data Availability

All data not published in this article will be shared on request from any qualified investigator.

Results

Genetic Investigations

We were unable to identify likely pathogenic variants by routine WES and WGS analyses described in the Methods section. Homozygosity mapping could not narrow down the homozygosity region shared in patients (eFigure 1, links.lww.com/NXG/A527). Considering REs, we used EHdn for genome-wide screening of REs in 2 patients (III-9 and III-11) compared with WGS data from 28 controls and found that ACAGG expansion at intron 2 of *RFC1* exhibited a top *p* value (0.01) among the candidate REs. Of interest, EHdn identified approximately 28 and 13 depth-normalized counts of anchored in-repeat reads in III-9 and III-11, respectively, raising the possibility of another repeat motif expansion in III-11. ExpansionHunter confirmed the ACAGG expansion in III-9 and III-11 (Figure 2A). Integral Genome Viewer showed a reduced read depth of WGS in this region (Figure 2B), and the soft-clipped read sequence in this region suggested AAGGG and ACAGG pentanucleotide repeats in affected III-9, ACAGG pentanucleotide repeats in affected III-11, and AAGGG pentanucleotide repeats in nonaffected III-12 (Figure 2C). Flanking PCR was unable to amplify any bands in all 6 patients and IV-10 with suspected disease status, suggesting biallelic REs, whereas all unaffected individuals had 1 allele of an intermediate RE (Figure 3A). No intermediate REs of pathologic repeat motifs have been found so far,[32] suggesting that such intermediate REs are probably REs of nonpathological repeat motifs. Expansion of repeats was confirmed by Southern blot hybridization analysis, except for 2 individuals (III-10 and III-12, Figure 3B). Determination of repeat motifs by RP-PCR indicated that III-1, III-11, and IV-9 had biallelic $(ACAGG)_{exp}$, and III-7, III-8, III-9, and IV-10

Table 1 Summary of Characteristics of Repeat Expansion in Family Members

Individual	Affected	Flanking PCR product	RP-PCR			Genotype	Repeating unit size
			AAGGG	ACAGG	AAAAG		
II-1	No	Intermediate expansion	−	+	+	$(ACAGG)_{exp}/(AAAAG)_{interexp}$	700, 80
II-6	No	Intermediate expansion	−	+	+	$(ACAGG)_{exp}/(AAAAG)_{interexp}$	1,900, 80
III-1	Yes	−	−	+	−	$(ACAGG)_{exp}/(ACAGG)_{exp}$	2,000, 800
III-7	Yes	−	+	+	−	$(AAGGG)_{exp}/(ACAGG)_{exp}$	2,100, 800
III-8	Yes	−	+	+	−	$(AAGGG)_{exp}/(ACAGG)_{exp}$	2,000, 600
III-9	Yes	−	+	+	−	$(AAGGG)_{exp}/(ACAGG)_{exp}$	2,000, 600
III-10	No	Intermediate expansion	+	−	+	$(AAGGG)_{exp}/(AAAAG)_{interexp}$	Undetermined
III-11	Yes	−	−	+	−	$(ACAGG)_{exp}/(ACAGG)_{exp}$	1,900, 800
III-12	No	Intermediate expansion	+	−	+	$(AAGGG)_{exp}/(AAAAG)_{interex}$	Undetermined
IV-9	Yes	−	−	+	−	$(ACAGG)_{exp}/(ACAGG)_{exp}$	1,900, 1,900
IV-10	Suspected	−	+	+	−	$(AAGGG)_{exp}/(ACAGG)_{exp}$	1,900, 700

Abbreviations: exp = expansion; interexp = intermediate expansion; RP-PCR = repeat-primed PCR.

had $(AAGGG)_{exp}$ and $(ACAGG)_{exp}$ in a compound heterozygous state (Figure 3C, Table 1, and eFigure 2). However, all unaffected individuals (II-1, II-6, III-10, and III-12) had 1 allele of the nonpathogenic intermediate $(AAAAG)_{exp}$, and 1 allele of pathogenic $(AAGGG)_{exp}$ and $(ACAGG)_{exp}$ in a compound heterozygous state (Table 1 and eFigure 2).

Haplotype Analysis

We selected informative variants from the WGS data and constructed the haplotypes associated with each repeat motif (eTable 1, links.lww.com/NXG/A527). Both the $(AAGGG)_{exp}$ and $(ACAGG)_{exp}$ motifs also shared the core ancestral haplotype described in previous reports[10,11] (eTable 1). In our cases, the $(ACAGG)_{exp}$ motif partially shared the haplotype of the Niue patient,[11] which is widely observed in non-European populations. The $(AAGGG)_{exp}$ motif partially shared the haplotype of Caucasian patients.[10] Notably, detailed analysis of core haplotypes revealed that each pathologic RE had different haplotypes, indicating that they arose from the 2 ancestors who independently developed $(AAGGG)_{exp}$ and $(ACAGG)_{exp}$ (Figure 1, eTables 2 and 3). These results suggest that although 2 pathologic REs arose from the same origin (shared core ancestral haplotype), the family under study might have 2 ancestors who independently developed $(AAGGG)_{exp}$ and $(ACAGG)_{exp}$.

Clinical Features

We summarized the symptoms of the patients in eTable 4 (links.lww.com/NXG/A527) and the comparison of the clinical manifestations for each genotype with previous reports in Table 2. We also show the brain MRI in Figure 4 and eFigure 3, ^{18}F-FDG PET in Figure 5, A and B, and SPECT in Figure 5C. All 6 patients but not VI-10 presented with ataxic gait at age 44–66 (average 57.7) years. IV-10 evaluated at age 52 years presented only with sensory neuropathy, not ataxic gait, and because she also had diabetes mellitus, it was difficult to distinguish whether the sensory neuropathy was caused by *RFC1* REs or diabetes mellitus. Many core symptoms of *RFC1*-related disorder,[15] including ataxia (7/8, 87.5%), sensory neuropathy (7/7, 100%), bilateral vestibulopathy (2/3, 66.7%), cough (5/7, 71.4%), and autonomic dysfunction (4/7, 57.1%), were commonly observed in this family. In addition, a variety of other rare symptoms were observed in the family. Atrophy and weakness of the distal muscles, suggesting motor neuropathy, were observed in 5 patients (5/7, 71.4%). Slightly irregular no-no head tremor at approximately 3 Hz in the sitting and standing positions was observed in 5 patients (5/7, 71.4%). In addition, parkinsonism was observed in 3 patients (3/7, 42.9%) and dystonia in 1 patient (1/7, 14.3%) (eFigure 4, A–C). III-8 and III-9 had obvious cognitive impairment and eventually had difficulty communicating. Cognitive function tests were performed for III-9, III-11, and IV-9. Although III-11 and IV-9 showed no obvious cognitive impairment, all 3 individuals showed a decline in the frontal assessment battery (FAB) compared with the Mini-Mental State Examination (MMSE) (eTable 4). MRIs of 7 individuals showed cerebellar atrophy in 6 cases, with IV-10 as the exception. Atrophy around the Sylvian fissure was characteristic of III-8 and III-9 (eFigure 3). VSRAD was performed in III-9, III-11, and IV-9. III-9 was characterized by atrophy of the gray matter of the cerebrum, especially around the Sylvian fissure, whereas III-11 was characterized by severe atrophy of the cerebellar gray matter without cerebral atrophy (Figure 4, A–C). ^{18}F-FDG PET performed on III-9 showed a strong decrease in glucose metabolism in the frontal lobe rather than in the cerebellum (Figure 5A). ^{18}F-FDG PET of III-11 and SPECT of IV-9 showed a decreased glucose metabolism and blood flow mainly in the cerebellum (Figure 5, B and C). The

Table 2 Comparison of Clinical Features

Genotype	$(ACAGG)_{exp}/(ACAGG)_{exp}$	$(AAGGG)_{exp}/(ACAGG)_{exp}$	$(AAGGG)_{exp}/(AAGGG)_{exp}$	$(AAGGG)_{exp}/(AAGGG)_{exp}$	$(ACAGG)_{exp}/(ACAGG)_{exp}$
Reference	Our report	Our report	Cortes et al.[41]	Traschütz et al.[15]	Scriba et al.[11] Tsuchiya et al.[39]
Total number	3	3	100	70	4
Average age at onset of ataxia, y	54	58.67	52	53	54.67
Last examination after onset of ataxia, y	17	13	11	NA	17
Cough, n (%)	1/3 (33.3)	3/3 (100)	64/100 (64)	46/64 (71.88)	4/4 (100)
Sensory symptom, n (%)	3/3 (100)	2/2 (100)	Abnormal pinprick lower limbs 74/100 (74)	61/61 (100)	1/1 (100)
Dysarthria, n (%)	3/3 (100)	3/3 (100)	40/100 (40)	44/67 (65.67)	3/3 (100)
Ataxic gait, n (%)	3/3 (100)	3/3 (100)	Unsteadiness 83/100 (83)	70/70 (100)	3/3 (100)
Nystagmus, n (%)	3/3 (100)	3/3 (100)	55/100 (55)	NA	1/1 (100)
Limb ataxia, n (%)	3/3 (100)	3/3 (100)	Abnormal finger-nose 49/100 (49) Abnormal heel-shin 52/100 (52)	Dysdiadochokinesia 44/62 (70.97)	1/1 (100)
Muscle atrophy, n (%)	3/3 (100)	2/3 (66.7)	NA	11/54 (20.37)	2/3 (66.67)
Muscle weakness, n (%)	3/3 (100)	2/3 (66.7)	0/100 (0)	3/54 (5.56)	2/3 (66.67)
Fasciculation, n (%)	1/3 (33.3)	0/3 (0)	NA	NA	3/3 (100)
Autonomic dysfunction, n (%)	1/3 (33.3)	3/3 (100)	32/100 (32)	39/63 (61.90)	1/1 (100)
Head tremor, n (%)	2/3 (66.7)	3/3 (100)	NA	NA	NA
Resting tremor, n (%)	2/3 (66.7)	1/3 (33.3)	NA	NA	NA
Bradykinesia, n (%)	2/3 (66.7)	1/3 (33.3)	NA	NA	NA
Cognitive impairment, n (%)	2/3 (66.7)	2/3 (66.7)	NA	13/52 (25)	NA
NCS, n (%)					
Small or absent SNAPs	2/2 (100)	3/3 (100)	100/100 (100)	42/42 (100)	3/3 (100)
Small CMAPs	2/2 (100)	1/3 (33.3)	2/100 (2)	Motor neuropathy 18/45 (40.0)	2/3 (66.67)
Brain MRI, n (%)					
Cerebellar atrophy	3/3 (100)	3/3 (100)	67/100 (67)	Vermal atrophy 48/55 (87.27) Hemispheric atrophy 33/47 (70.21)	3/3 (100)
Cerebral atrophy	1/3 (33.3)	2/3 (66.7)	19/100 (19)	20/55 (37)	NA

Abbreviations: CMAP = compound muscle action potential; NA = not available; NCS = nerve conduction study; SNAP = sensory nerve action potential.

detailed medical history of representative cases III-9 and IV-9 is presented in the Supplemental Material.

Discussion

Our study clearly demonstrated the utility of WGS and RE detection tools for genetic diagnosis of a family with hereditary SCD, in which candidate genes could not be narrowed down because of a complex family structure and atypical clinical presentation. Individuals with *RFC1*-related disorders present with a wide spectrum of symptoms, and it is often difficult to suspect the disease when symptoms are few in the early stages or when the disease presents with many atypical symptoms, as in this family under study. For patients with SCA, after fragment analysis for some representative repeat disorders, targeted resequencing panel or exome analysis is sometimes performed,[1] but the diagnostic rates of targeted resequencing panels and exome analysis are reported to be as low as 17% and 36%, respectively.[33] One possible reason for this low diagnostic

Figure 4 MRIs Analyzed by VSRAD

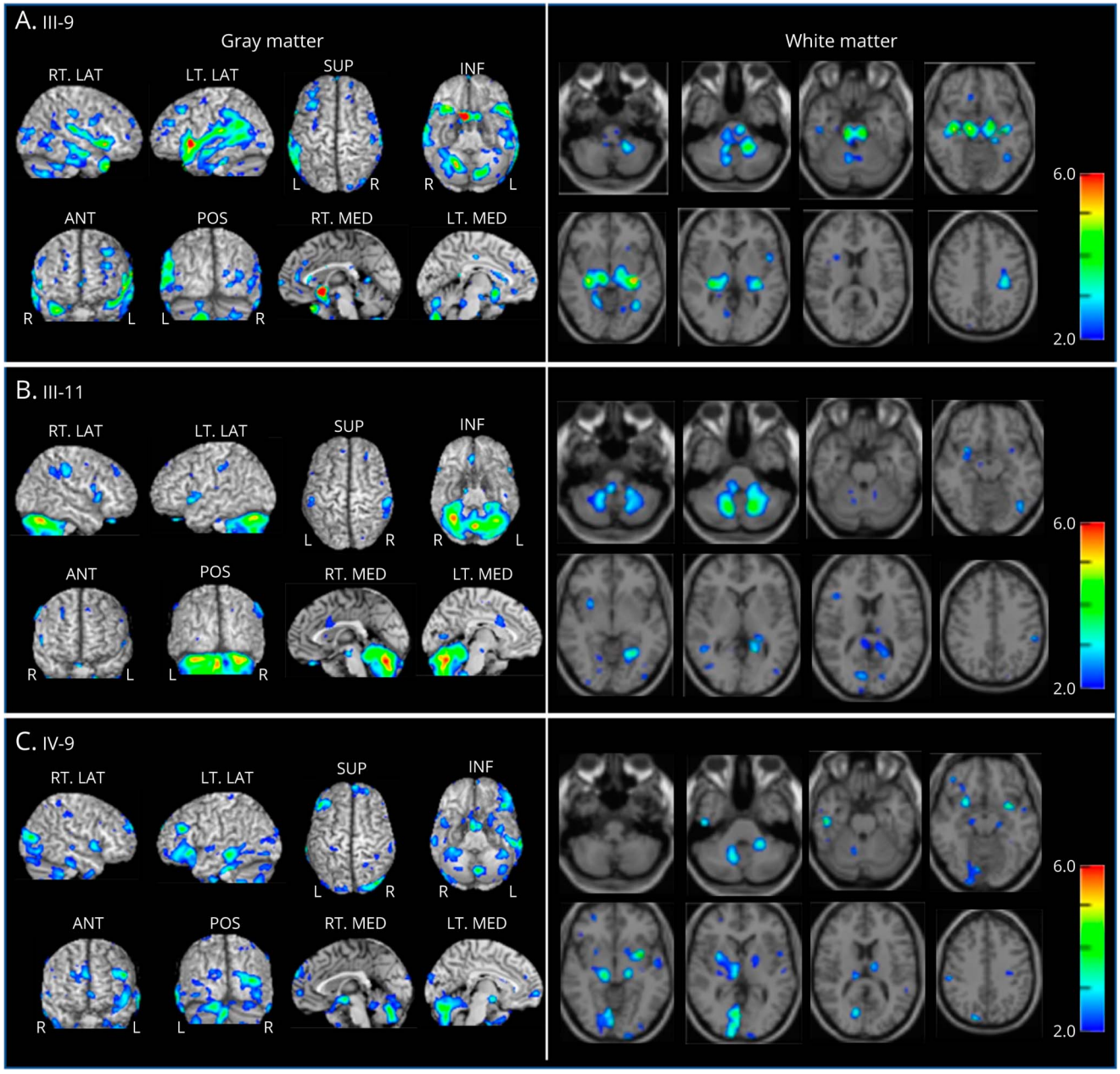

MRIs of III-9 at age 77 years (A), III-11 at age 75 years (B), and IV-9 at age 57 years (C), analyzed using VSRAD. Z-score maps displayed on an anatomically standardized MRI template are shown. (A) In III-9, atrophy of the cerebral gray matter around the Sylvian fissure, part of the frontal lobe, and part of the cerebellum, as well as atrophy of the white matter in the cerebellum, brainstem, and thalamus, were observed. (B) In III-11, strong cerebellar gray matter atrophy and cerebellar white matter atrophy were observed, but little cerebral atrophy was detected. (C) Atrophy of the cerebellar gray and white matter and mild atrophy of the cerebral gray matter were observed in IV-9. VSRAD = voxel-based specific regional analysis system for Alzheimer disease.

rate is that hereditary SCD includes many disorders caused by REs. In Japan, SCA3 and SCA6 are the most common causes of autosomal dominant SCD, as is the trend worldwide, but SCA31 and dentatorubral-pallidoluysian atrophy, which are rare in Western countries, are more common in Japan, whereas SCA1 and SCA2 are relatively rare.[34,35] As rare diseases, there are reports of RE diseases resulting from intronic REs such as SCA10[36] and SCA36.[37] In autosomal recessive SCD, Friedreich ataxia is common in Western countries but has not been reported in Japan. Although it has been reported that *RFC1*-related disease is not a rare disease in Western countries, the prevalence of *RFC1*-related disease in Japan has not yet been reported. However, several cases of *RFC1*-related disease have been reported in Japan[38,39]; thus, *RFC1*-related disease may not be a rare disease. The use of WGS and repeat detection tools is very simple and would increase the detection rate of rare repeat disorders that might be overlooked in targeted resequencing panels and exome analysis.

Figure 5 Analysis of Brain Metabolism and Blood Flow Using SPECT or ^{18}F-FDG-PET

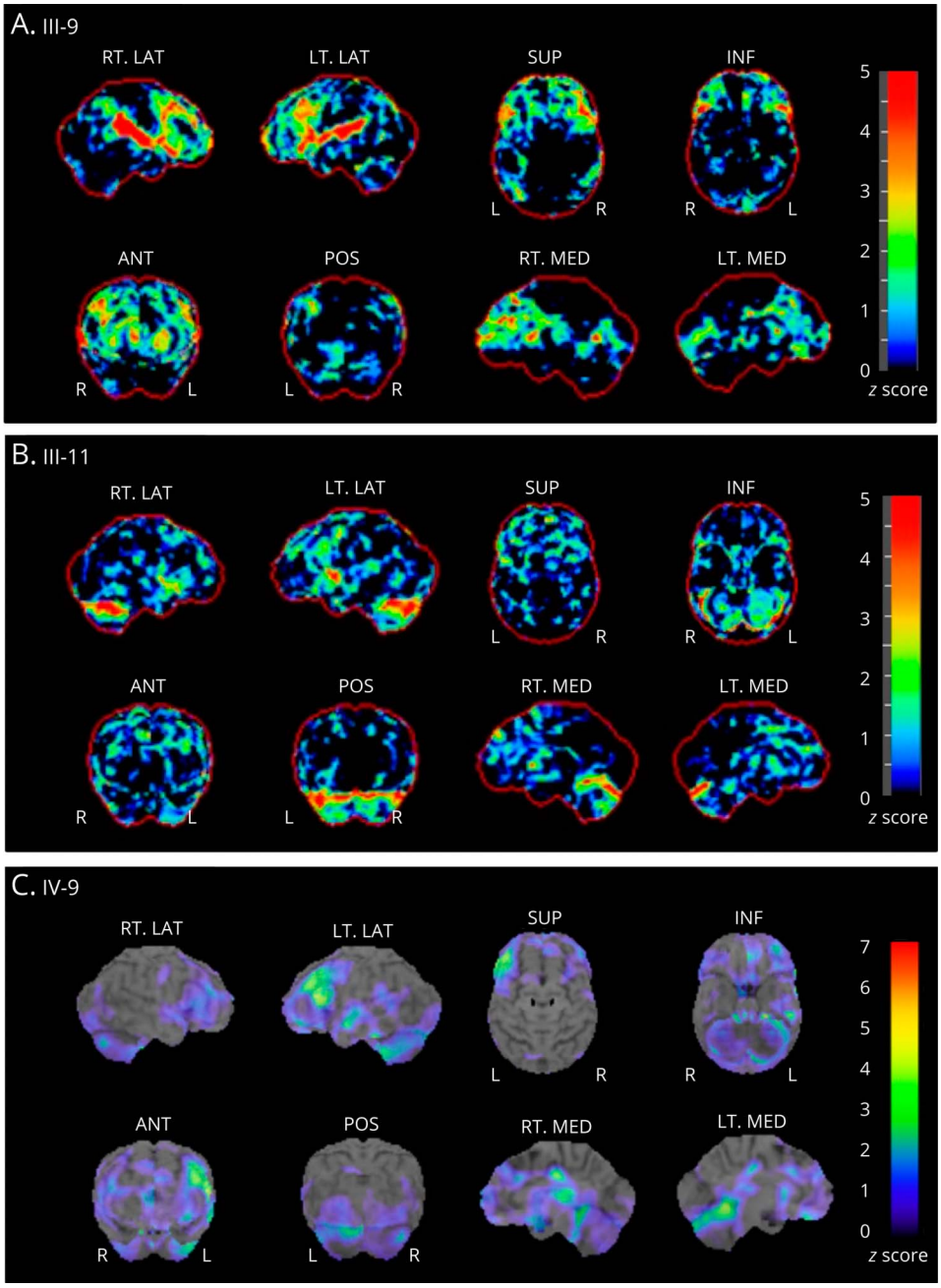

(A and B) ^{18}F-FDG PET results of III-9 (A) and III-11 (B). Z-score maps of reduced uptake of ^{18}F-FDG by anatomically standardized brain are shown. (A) A strong decreased glucose metabolism around the Sylvian fissure and in the frontal lobe was observed in III-9. (B) A strongly decreased glucose metabolism in the cerebellum was observed in III-11. (C) ^{123}I-IMP SPECT imaging of IV-9. Z-score maps displayed on an anatomically standardized MRI template are shown. Decreased blood flow in the cerebellum and frontal lobe was observed in IV-9. ^{123}I-IMP = N-isopropyl-^{123}I-ρ-iodoamphetamine; 18F-FDG = 18F-fluorodeoxyglucose.

There are a variety of repeat motifs in REs of *RFC1* intron 2,[10,11,40] but only 2 motifs, AAGGG and ACAGG, have been known to cause *RFC1*-related disorders. Most cases of *RFC1*-related disorders, especially in Europe, have biallelic $(AAGGG)_{exp}$, whereas only 4 cases in 3 families of the Asian-Pacific area have been reported to have biallelic $(ACAGG)_{exp}$.[11,39] Our family included 3 patients and a suspected case (IV-10) with $(AAGGG)_{exp}$ and $(ACAGG)_{exp}$ in a compound heterozygous state and 3 patients with biallelic $(ACAGG)_{exp}$. To compare the clinical symptoms for each genotype, we summarized our cases, 2 large cohort studies of *RFC1*-related disorder with biallelic $(AAGGG)_{exp}$, and previously reported cases of biallelic $(ACAGG)_{exp}$ (Table 2). IV-10 was not included in this comparison. The core symptoms of *RFC1*-related disorders, such as ataxia, sensory neuropathy, and cough, appear to be indistinguishable between each genotype. Vestibular dysfunction should also be considered, but in our cases, the examination was insufficient, and no comparison could be made. Atrophy and muscle weakness of distal muscles, indicating motor neuropathy, were more common in patients with $(AAGGG)_{exp}$ and $(ACAGG)_{exp}$ in compound heterozygous state (66.7%, 66.7%) and patients with biallelic $(ACAGG)_{exp}$ (100%, 100%)

than in patients with biallelic $(AAGGG)_{exp}$ (not available, 0%[41] and 20.37%, 5.56%[15]). It has been reported that biallelic $(ACAGG)_{exp}$ cases are characterized by muscular atrophy and fasciculation due to motor neuropathy,[11] and the results obtained for the family under study were consistent with this report.

In the family under study, involuntary movements, such as head tremor, laryngeal dystonia, and striatal foot, were observed. A study reported 6 of 57 RFC1-related disorder patients presented with involuntary movements (oral-facial dyskinesia, oral-facial dystonia or chorea of the extremities).[15] Furthermore, a patient in this study exhibited head tremors as a symptom, similar to that observed in patients of the present study; thus, head tremors were subsequently considered to be one of the symptoms of *RFC1*-related disorder. In our family, involuntary movements were one of the reasons why *RFC1*-related disorders were not initially considered a causative disease, and it should be known that patients with *RFC1*-related disorders can present with a variety of involuntary movements.

In the family under study, some patients presented with cognitive impairment and cerebral atrophy. A report showed that 25% of *RFC1*-related disorders were complicated by cognitive impairment,[15] and another showed that 2 of 4 patients with *RFC1*-related disorder had decreased MMSE or FAB.[16] Cerebral atrophy with parietal lobe predominance has previously been found in 37% of patients with *RFC1*-related disorders.[15] A study analyzed brain volumes of patients with *RFC1*-related disorder and reported widespread and relatively symmetric atrophy of the cerebellum and basal ganglia, atrophy of the brain stem, and atrophy of the cerebral white matter, mainly in the corpus callosum and deep corridors, whereas damage to the cerebral cortex was limited.[42]

To investigate in detail the cognitive impairment of RFC1-related disorders, we examined the relationship between brain atrophy, metabolic or blood flow changes, and cognitive impairment. In our cases, 2 patterns of brain atrophy and metabolic or blood flow changes were observed: cerebral dominant and cerebellar dominant. III-9 showed perisylvian atrophy and metabolic changes, and III-8 showed only perisylvian atrophy. III-11 and IV-9 showed atrophy and metabolic or blood flow changes, mainly in the cerebellum. However, regardless of the pattern of brain atrophy and metabolic or blood flow changes, cognitive function tests were characterized by stronger impairment in the FAB compared with the MMSE. III-9 clearly showed stronger atrophy and metabolic changes of the frontal lobe than the cerebellum, suggesting that frontal lobe metabolic changes were largely responsible for cognitive impairment. However, III-11 and IV-9 showed cognitive impairment in cognitive function tests without obvious cerebral metabolic or blood flow changes, suggesting that factors other than cerebral metabolic or blood flow changes may be related to cognitive impairment. Cognitive dysfunction caused by cerebellar disorders, which is called cerebellar cognitive affective syndrome (CCAS),[43] has been revealed in recent years, and because III-9 has particularly strong cerebellar atrophy, CCAS is considered one of the possible causes of cognitive impairment. The degree of cerebral damage varies widely, even within the same family, and in some cases, cerebral damage was stronger than cerebellar damage and was thought to be the cause of cognitive impairment. Considering that cortical damage has been reported to be mild in RFC1-related disorders in the previous report,[42] the ACAGG allele may be prone to show a variety of phenotypes of cortical damage. However, only 1 case was proved to have severe cortical damage, and whether the ACAGG allele is associated with cortical symptoms needs to be further investigated.

A previous study reported that there was no association between age at onset and the number of AAGGG repeat units on either the smaller or larger allele.[10] In our family, III-1, III-7, III-8, III-9, and III-11, in whom the larger expansion allele had about 2000 repeats and the smaller allele about 600–800 repeats, presented ataxia in their late 50s. In contrast, IV-9, in which both alleles had about 1900 repeats, developed ataxia at age 44 years, indicating an earlier onset than the other family members. In this family, the number of repeats of the 2 alleles may be related to the age at onset of ataxia. However, this study included a small number of cases, and thus, this finding needs to be examined in a larger number of cases.

Previous studies have reported that patients with $(AAGGG)_{exp}$ shared the same core haplotype as in the Caucasian cohort[10] and that the core haplotype was also shared by other non-Caucasian patients with *RFC1*-related disorder.[38,44] These results suggest that the $(AAGGG)_{exp}$ has a single origin, most likely in Europe.[10] Furthermore, it was reported that patients with the $(ACAGG)_{exp}$ shared the same core haplotype as those with $(AAGGG)_{exp}$ in the Asian-Pacific CANVAS cohort.[11] These findings suggest that $(ACAGG)_{exp}$ also originates from the same origin as the $(AAGGG)_{exp}$.[11] However, in the current family under study, a detailed examination of the informative variants between the core haplotypes revealed that the $(AAGGG)_{exp}$ and $(ACAGG)_{exp}$ had different haplotypes (Figure 1 and eTable 3, links.lww.com/NXG/A527). Homozygosity mapping also did not detect homozygous regions in the corresponding area. Considering these findings, we suggest a novel hypothesis that these 2 pathologic REs have likely originated from independent ancestors.

We have shown that WGS and repeat detection tools are very effective for comprehensive genetic testing in SCD. Our *RFC1*-related disease family included patients with $(ACAGG)_{exp}$ and $(AAGGG)_{exp}$ in a compound heterozygous state, which were characterized by motor neuropathy and patients with homozygous $(ACAGG)_{exp}$. Brain imaging suggested frontal lobe predominant cortical metabolic changes to be the likely cause of cognitive impairment in one case with *RFC1*-related disorders, whereas others presented with cognitive impairment but no noticeable metabolic or blood flow changes in the cerebrum. Because we have studied only a small number of patients, the relationship between genotype

and symptoms, as well as cerebral metabolic or blood flow changes and cognitive impairment, needs to be further examined in more individuals.

Acknowledgment

The authors thank the patient's family for participating in this study. They also thank Prof. K. Yoshiura (Department of Human Genetics, Atomic Bomb Disease Institute, Nagasaki University, Nagasaki, Japan) for his technical advices. The authors thank Editage (editage.com) for English language editing.

Study Funding

This work was supported by Grant-in-Aid from the Ministry of Health, Labour and Welfare of Japan Grants-in-Aid for Scientific Research (B) (JP20H03641) and (C) (JP20K08236) from the Japan Society for the Promotion of Science, the Takeda Science Foundation HUSM Grant-in-Aid from Hamamatsu University School of Medicine.

Disclosure

The authors report no disclosures. Go to Neurology.org/NG for full disclosures.

Publication History

Received by *Neurology: Genetics* November 21, 2021. Accepted in final form April 7, 2022.

Appendix Authors

Name	Location	Contribution
Kazuki Watanabe, MD	Department of Biochemistry, and Department of Neurology, Hamamatsu University School of Medicine, Hamamatsu, Japan	Drafting/revision of the manuscript for content, including medical writing for content; major role in the acquisition of data; study concept or design; and analysis or interpretation of data
Mitsuko Nakashima, MD, PhD	Department of Biochemistry, Hamamatsu University School of Medicine, Hamamatsu, Japan	Drafting/revision of the manuscript for content, including medical writing for content, and analysis or interpretation of data
Rie Wakatsuki, MD	Department of Neurology, Hamamatsu University School of Medicine, Hamamatsu, Japan	Drafting/revision of the manuscript for content, including medical writing for content, and major role in the acquisition of data
Tomoyasu Bunai, MD, PhD	Department of Neurology, and Department of Biofunctional Imaging, Hamamatsu University School of Medicine, Hamamatsu, Japan	Drafting/revision of the manuscript for content, including medical writing for content, and analysis or interpretation of data
Yasuomi Ouchi, MD, PhD	Department of Biofunctional Imaging, Hamamatsu University School of Medicine, Hamamatsu, Japan	Drafting/revision of the manuscript for content, including medical writing for content, and analysis or interpretation of data
Tomohiko Nakamura, MD, PhD	Department of Neurology, Hamamatsu University School of Medicine, Hamamatsu, Japan	Drafting/revision of the manuscript for content, including medical writing for content, and analysis or interpretation of data
Hiroaki Miyajima, MD, PhD	Department of Neurology, Hamamatsu University School of Medicine, Hamamatsu, Japan	Drafting/revision of the manuscript for content, including medical writing for content, and analysis or interpretation of data
Hirotomo Saitsu, MD, PhD	Department of Biochemistry, Hamamatsu University School of Medicine, Hamamatsu, Japan	Drafting/revision of the manuscript for content, including medical writing for content; study concept or design; and analysis or interpretation of data

References

1. Sullivan R, Yau WY, O'Connor E, Houlden H. Spinocerebellar ataxia: an update. *J Neurol*. 2019;266(2):533-544.
2. Sone J, Mitsuhashi S, Fujita A, et al. Long-read sequencing identifies GGC repeat expansions in NOTCH2NLC associated with neuronal intranuclear inclusion disease. *Nat Genet*. 2019;51(8):1215-1221.
3. Gorcenco S, Ilinca A, Almasoudi W, Kafantari E, Lindgren AG, Puschmann A. New generation genetic testing entering the clinic. *Parkinsonism Relat Disord*. 2020;73:72-84.
4. Rafehi H, Szmulewicz DJ, Bennett MF, et al. Bioinformatics-based identification of expanded repeats: a non-reference intronic pentamer expansion in RFC1 causes CANVAS. *Am J Hum Genet*. 2019;105(1):151-165.
5. Rafehi H, Szmulewicz DJ, Pope K, et al. Rapid diagnosis of spinocerebellar ataxia 36 in a three-generation family using short-read whole-genome sequencing data. *Mov Disord*. 2020;35(9):1675-1679.
6. Corbett MA, Kroes T, Veneziano L, et al. Intronic ATTTC repeat expansions in STARD7 in familial adult myoclonic epilepsy linked to chromosome 2. *Nat Commun*. 2019;10(1):4920.
7. Ishiura H, Shibata S, Yoshimura J, et al. Noncoding CGG repeat expansions in neuronal intranuclear inclusion disease, oculopharyngodistal myopathy and an overlapping disease. *Nat Genet*. 2019;51(8):1222-1232.
8. Bronstein AM, Mossman S, Luxon LM. The neck-eye reflex in patients with reduced vestibular and optokinetic function. *Brain*. 1991;114(pt 1A):1-11.
9. Migliaccio AA, Halmagyi GM, McGarvie LA, Cremer PD. Cerebellar ataxia with bilateral vestibulopathy: description of a syndrome and its characteristic clinical sign. *Brain*. 2004;127(pt 2):280-293.
10. Cortese A, Simone R, Sullivan R, et al. Biallelic expansion of an intronic repeat in RFC1 is a common cause of late-onset ataxia. *Nat Genet*. 2019;51(4):649-658.
11. Scriba CK, Beecroft SJ, Clayton JS, et al. A novel RFC1 repeat motif (ACAGG) in two Asia-Pacific CANVAS families. *Brain*. 2020;143(10):2904-2910.
12. Wan L, Chen Z, Wan N, et al. Biallelic intronic AAGGG expansion of RFC1 is related to multiple system Atrophy. *Ann Neurol*. 2020;88(6):1132-1143.
13. Sullivan R, Yau WY, Chelban V, et al. RFC1-related ataxia is a mimic of early multiple system atrophy. *J Neurol Neurosurg Psychiatry*. 2021;92(4):444-446.
14. da Silva Schmitt G, Martinez ARM, da Graça FF, et al. Dopa-responsive Parkinsonism in a patient with homozygous RFC1 expansions. *Mov Disord*. 2020;35(10):1889-1890.
15. Traschütz A, Cortese A, Reich S, et al. Natural history, phenotypic spectrum, and discriminative features of multisystemic RFC1 disease. *Neurology*. 2021;96(9):e1369-e1382.
16. Herrmann L, Gelderblom M, Bester M, et al. Multisystemic neurodegeneration caused by biallelic pentanucleotide expansions in *RFC1*. *Parkinsonism Relat Disord*. 2022;95:54-56.
17. Human genetic variation database. Accessed November 11, 2011. hgvd.genome.med.kyoto-u.ac.jp/.
18. 8.3KJPN. Accessed November 11, 2011. jmorp.megabank.tohoku.ac.jp/202102/downloads/legacy/.
19. gnomAD. Accessed November 11, 2011. gnomad.broadinstitute.org/.
20. Ng PC, Henikoff S. SIFT: predicting amino acid changes that affect protein function. *Nucleic Acids Res*. 2003;31(13):3812-3814.
21. Adzhubei IA, Schmidt S, Peshkin L, et al. A method and server for predicting damaging missense mutations. *Nat Methods*. 2010;7(4):248-249.
22. Schwarz JM, Cooper DN, Schuelke M, Seelow D. MutationTaster2: mutation prediction for the deep-sequencing age. *Nat Methods*. 2014;11(4):361-362.

23. Kircher M, Witten DM, Jain P, O'Roak BJ, Cooper GM, Shendure J. A general framework for estimating the relative pathogenicity of human genetic variants. *Nat Genet*. 2014;46(3):310-315.
24. Fromer M, Moran JL, Chambert K, et al. Discovery and statistical genotyping of copy-number variation from whole-exome sequencing depth. *Am J Hum Genet*. 2012;91(4):597-607.
25. Nord AS, Lee M, King MC, Walsh T. Accurate and exact CNV identification from targeted high-throughput sequence data. *BMC Genomics*. 2011;12:184.
26. Roller E, Ivakhno S, Lee S, Royce T, Tanner S. Canvas: versatile and scalable detection of copy number variants. *Bioinformatics*. 2016;32(15):2375-2377.
27. Chen X, Schulz-Trieglaff O, Shaw R, et al. Manta: rapid detection of structural variants and indels for germline and cancer sequencing applications. *Bioinformatics*. 2016;32(8):1220-1222.
28. Thung DT, de Ligt J, Vissers LE, et al. Mobster: accurate detection of mobile element insertions in next generation sequencing data. *Genome Biol*. 2014;15(10):488.
29. HomozygosityMapper. Accessed November 11, 2011. teufelsberg.charite.de/HomozygosityMapper/.
30. Dolzhenko E, Bennett MF, Richmond PA, et al. ExpansionHunter Denovo: a computational method for locating known and novel repeat expansions in short-read sequencing data. *Genome Biol*. 2020;21(1):102.
31. Dolzhenko E, van Vugt J, Shaw RJ, et al. Detection of long repeat expansions from PCR-free whole-genome sequence data. *Genome Res*. 2017;27(11):1895-1903.
32. Aboud Syriani D, Wong D, Andani S, et al. Prevalence of RFC1-mediated spinocerebellar ataxia in a North American ataxia cohort. *Neurol Genet*. 2020;6(3):e440.
33. Galatolo D, Tessa A, Filla A, Santorelli FM. Clinical application of next generation sequencing in hereditary spinocerebellar ataxia: increasing the diagnostic yield and broadening the ataxia-spasticity spectrum. A retrospective analysis. *Neurogenetics*. 2018;19(1):1-8.
34. Basri R, Yabe I, Soma H, Sasaki H. Spectrum and prevalence of autosomal dominant spinocerebellar ataxia in Hokkaido, the northern island of Japan: a study of 113 Japanese families. *J Hum Genet*. 2007;52(10):848-855.
35. Nozaki H, Ikeuchi T, Kawakami A, et al. Clinical and genetic characterizations of 16q-linked autosomal dominant spinocerebellar ataxia (AD-SCA) and frequency analysis of AD-SCA in the Japanese population. *Mov Disord*. 2007;22(6):857-862.
36. Naito H, Takahashi T, Kamada M, et al. First report of a Japanese family with spinocerebellar ataxia type 10: the second report from Asia after a report from China. *PLoS One*. 2017;12(5):e0177955.
37. Kobayashi H, Abe K, Matsuura T, et al. Expansion of intronic GGCCTG hexanucleotide repeat in NOP56 causes SCA36, a type of spinocerebellar ataxia accompanied by motor neuron involvement. *Am J Hum Genet*. 2011;89(1):121-130.
38. Nakamura H, Doi H, Mitsuhashi S, et al. Long-read sequencing identifies the pathogenic nucleotide repeat expansion in RFC1 in a Japanese case of CANVAS. *J Hum Genet*. 2020;65(5):475-480.
39. Tsuchiya M, Nan H, Koh K, et al. RFC1 repeat expansion in Japanese patients with late-onset cerebellar ataxia. *J Hum Genet*. 2020;65(12):1143-1147.
40. Akçimen F, Ross JP, Bourassa CV, et al. Investigation of the RFC1 repeat expansion in a Canadian and a Brazilian ataxia cohort: identification of novel conformations. *Front Genet*. 2019;10:1219.
41. Cortese A, Tozza S, Yau WY, et al. Cerebellar ataxia, neuropathy, vestibular areflexia syndrome due to RFC1 repeat expansion. *Brain*. 2020;143(2):480-490.
42. Matos P, Rezende TJR, Schmitt GS, et al. Brain structural signature of RFC1-related disorder. *Mov Disord*. 2021;36(11):2634-2641.
43. Argyropoulos GPD, van Dun K, Adamaszek M, et al. The cerebellar cognitive affective/Schmahmann syndrome: a task force paper. *Cerebellum*. 2020;19(1):102-125.
44. Beecroft SJ, Cortese A, Sullivan R, et al. A Māori specific RFC1 pathogenic repeat configuration in CANVAS, likely due to a founder allele. *Brain*. 2020;143(9):2673-2680.